

# Ultraminiaturized High-Speed Permanent-Magnet Generators for Milliwatt-Level Power Generation

Florian Herrault, Chang-Hyeon Ji, and Mark G. Allen, *Senior Member, IEEE*

**Abstract**—This paper presents the design, fabrication, and characterization of millimeter-scale rotary electromagnetic generators. The axial-flux synchronous machines consist of a three-phase microfabricated surface-wound copper coil and a multipole permanent-magnet (PM) rotor measuring 2 mm in diameter. Several machines with various geometries and numbers of magnetic poles and turns per pole are designed and compared. Moreover, the use of different PM materials is investigated. Multipole magnetic rotors are modeled using finite element analysis to analyze magnetic field distributions. In operation, the rotor is spun above the microfabricated stator coils using an off-the-shelf air-driven turbine. As a result of design choices, the generators present different levels of operating frequency and electrical output power. The four-pole six-turn/pole NdFeB generator exhibits up to 6.6 mW<sub>rms</sub> of ac electrical power across a resistive load at a rotational speed of 392 000 r/min. This milliwatt-scale power generation indicates the feasibility of such ultrasmall machines for low-power applications. [2008-0078]

**Index Terms**—AC generators, micromachining, permanent-magnet (PM) machines, power microelectromechanical systems (MEMS).

## I. INTRODUCTION

THE NEED for ultracompact power sources is increasing as current electronic devices are becoming smaller and more energy demanding. This has driven the development of microelectromechanical systems (MEMS)-based permanent-magnet (PM) generators, which are potentially very attractive as mechanical-to-electrical transducers in small power generation systems with output power ranging from a milliwatt to tens of watts. Appropriate mechanical input for microfabricated rotary PM generators can be provided via high-pressure gas sources [1]–[3] or microgas engines [4]. Over the past decade, progress has been made to achieve more compact high power density generators using MEMS technologies.

Holmes *et al.* fabricated 7.5-mm-diameter axial-flux PM generators, which consisted of an electroplated copper coil and a ball-bearing-supported SU-8 rotor with embedded

neodymium iron boron (NdFeB) magnets. At a rotational speed of 30 000 r/min, an open-circuit voltage of 0.42 V<sub>rms</sub> was measured, corresponding to a predicted output power of 1.1 mW across a resistive load. Basic scaling laws of electromagnetic machines were also presented [5]. Raisigel *et al.* developed 8-mm-diameter microfabricated planar generators. At a rotor speed of 380 000 r/min, the machines exhibited a maximum open-circuit voltage of 4.18 V<sub>rms</sub> and a measured output power of 5 W across a Y-connected resistance bridge. The generators consisted of a three-phase electroplated copper coil on a silicon substrate and a PM disk rotor [3]. Although the fabrication of 3-mm-diameter stators had been mentioned, no experimental data have been reported yet. Pan *et al.* reported 5-mm-diameter rotary electromagnetic PM generators using a unique fabrication approach for the stator that consists of winding and embedding a filament copper wire onto a substrate. Discrete NdFeB pieces were used for the PM rotor. At a rotational speed of 2200 r/min, a voltage of 0.079 V<sub>rms</sub> was measured in open circuit, which corresponds to a maximum power output of 0.41 mW [6]. Arnold recently reviewed the advances in microscale magnetic power generation systems, among which PM microgenerators were discussed [7].

Further miniaturization of these devices presents many challenges. As the scale decreases, several key parameters must be considered to maintain the output power at a practical level, such as low winding resistances, high rotational speeds, small air gaps, and magnetic degradation of small-scale PMs. Such effects and limitations have not been explored in miniaturized generators that have diameters of less than 5 mm, as confirmed by Arnold [7]. Previously, we reported 10-mm-diameter microfabricated PM generators that delivered an open-circuit voltage of 1.6 V<sub>rms</sub> and 8 W of dc power across a resistive load at a rotational speed of 305 000 r/min [8]. In contrast to other machines, the stator coil was microfabricated onto a NiFeMo ferromagnetic substrate to increase the magnetic flux of the machine and, thus, the output power [1], [2]. As noted therein, the use of an electrically conductive bulk substrate generates important eddy current losses in the stator core. A lamination scheme could reduce these eddy currents, resulting in the potential for increased mechanical-to-electrical power conversion efficiency. Furthermore, stress-related failures of high-speed rotors (> 100 000 r/min) were modeled and experimentally validated [9]. More recently, we investigated the ultraminiaturization of such PM generators. We reported the fabrication and measurement results of 2-mm-diameter two-pole ultraminiaturized NdFeB machines, which delivered up to 0.051 V<sub>rms</sub> in open circuit at a rotational speed of 392 000 r/min [10]. Actual power measurements were not performed.

Manuscript received March 24, 2008; revised June 18, 2008. First published November 7, 2008; current version published December 4, 2008. This paper was presented in part at the 14th International Conference on Solid-State Sensors, Actuators, and Microsystems, Lyon, France, June 2007. Subject Editor M. Wong.

F. Herrault is with l'Ecole Doctorale, Toulouse, France and also with the School of Electrical and Computer Engineering, Georgia Institute of Technology, Atlanta, GA 30332 USA (e-mail: fh59@mail.gatech.edu).

C.-H. Ji and M. G. Allen are with the School of Electrical and Computer Engineering, Georgia Institute of Technology, Atlanta, GA 30332 USA (e-mail: cji6@mail.gatech.edu; mark.allen@ece.gatech.edu).

Color versions of one or more of the figures in this paper are available online at <http://ieeexplore.ieee.org>.

Digital Object Identifier 10.1109/JMEMS.2008.2004854

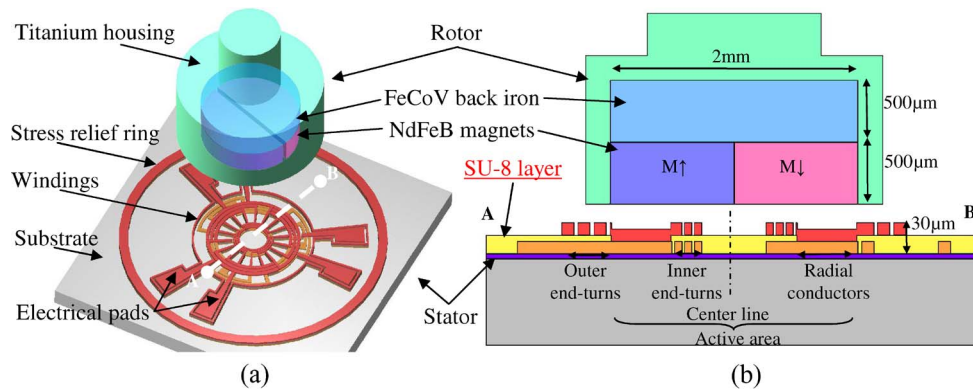


Fig. 1. Conceptual drawings of ultraminiaturized axial-flux rotary PM generators (two poles and three turns/pole). (a) Perspective view and (b) cross section A-B. The SU-8 insulating layer is not shown in (a) for design clarity.

This paper focuses on the ultraminiaturized multipole generators for milliwatt-level power generation. Based on a rotor diameter of 2 mm, we fabricated machines having various numbers of magnetic poles (two, four, and eight) and turns per pole (three and six), in order to explore tradeoffs in machine designs and performance. Magnetic simulations were carried out, and the fabricated generators were tested.

First, an overview of the generators is presented, followed by the constraints and benefits of miniaturization. Several different types of machine designs are reported and modeled using finite element analysis. Next, the fabrication of the devices is described, including stator microfabrication, PM machining, and rotor assembly. Measurements of the open-circuit voltage and the ac electrical power across a load resistance are reported. The performances of these various machines are finally discussed.

## II. PM MACHINE DESIGN

The generators are three-phase axial-flux multipole synchronous PM machines consisting of a rotor with a multipole PM and a ferromagnetic back iron, and a stator with electroplated surface-wound copper coils on a silicon substrate, as shown in Fig. 1. In Fig. 1(b), the thicknesses of the stator layers have been exaggerated for better clarity. The 2-mm-diameter multipole spinning rotor induces ac voltages in the stator windings by generating a time-varying magnetic field (Faraday's law). When the winding terminals are connected to an external load, the device generates electrical power.

### A. Miniaturization Constraints and Benefits

The key design concern in such small electromagnetic machines is to minimize the degradation of the magnetic performance, particularly in multipole magnetic rotors. As the overall size of the machine decreases, dimensions such as the air gap between the rotor and stator and the magnetization uniformity in the pole pieces start to significantly reduce the output power of the devices. Although the fabrication of ultraminiaturized stator windings benefits from microfabrication processes, it is still challenging to make millimeter-scale high-performance PM pieces.

First, each PM piece is used for one magnetic pole. The laser machining process used to shape the magnets causes some material degradation at the edges of the pieces, resulting in non-

magnetic regions typically a few hundred micrometers in width. Furthermore, imperfect shapes and rough edges cause slight gaps between the pole pieces. These fabrication limitations increase the lateral extent of the transition regions between two opposite magnetic poles (also called "dead zones"), which do not contribute to the magnetic flux. Because of the small size of the magnets, this may represent a nonnegligible percentage of the total area and thus decrease the performance of the machine.

Second, the magnetic flux captured by the stator windings comes from the fringing field between the opposite magnetic poles, as there is no ferromagnetic stator back iron to attract the flux toward the windings. Therefore, as the number of poles increases, the vertical component of the magnetic field intensity becomes smaller and thus reduces the total effective flux of the machine. As a result of these considerations, reducing the number of magnetic poles minimizes the degradation of the magnetic performance in these small-scale PM rotors.

With regard to the stator coil design, several factors have to be considered in order to maximize the output power. Surface-wound stator coils offer fabrication simplicity when compared to their fully 3-D counterparts; however, even these coils can suffer from microfabrication-related limitations such as photoresist aspect ratio, number of copper layers, and limited cross-sectional area of the windings. As a result, tradeoffs between the number of turns and the resistance of the windings have to be investigated at the microscale.

Basic scaling laws for electromagnetic rotational machines have been previously reported [5]. Theoretically, the power density remains constant as the size decreases, if the tip speed of the rotor is maintained constant. Consequently, such machines are very attractive for small-scale technologies. In addition, the downscaling of electrical generators provides other advantages such as significant reduction of the volume and mass of power sources.

As a consequence, small-scale generators require higher rotational speeds in order to provide higher output power. However, higher rotational speeds induce higher mechanical stress in the rotating system, which is one of the main drawbacks of such machines. Failure mechanisms and analytical calculations of high-speed PM rotors have been previously presented [9]. Since peak radial stress is proportional to the square of the rotor diameter, PM rotary generators could benefit greatly from scale reduction. Experimentally, 10-mm-diameter samarium

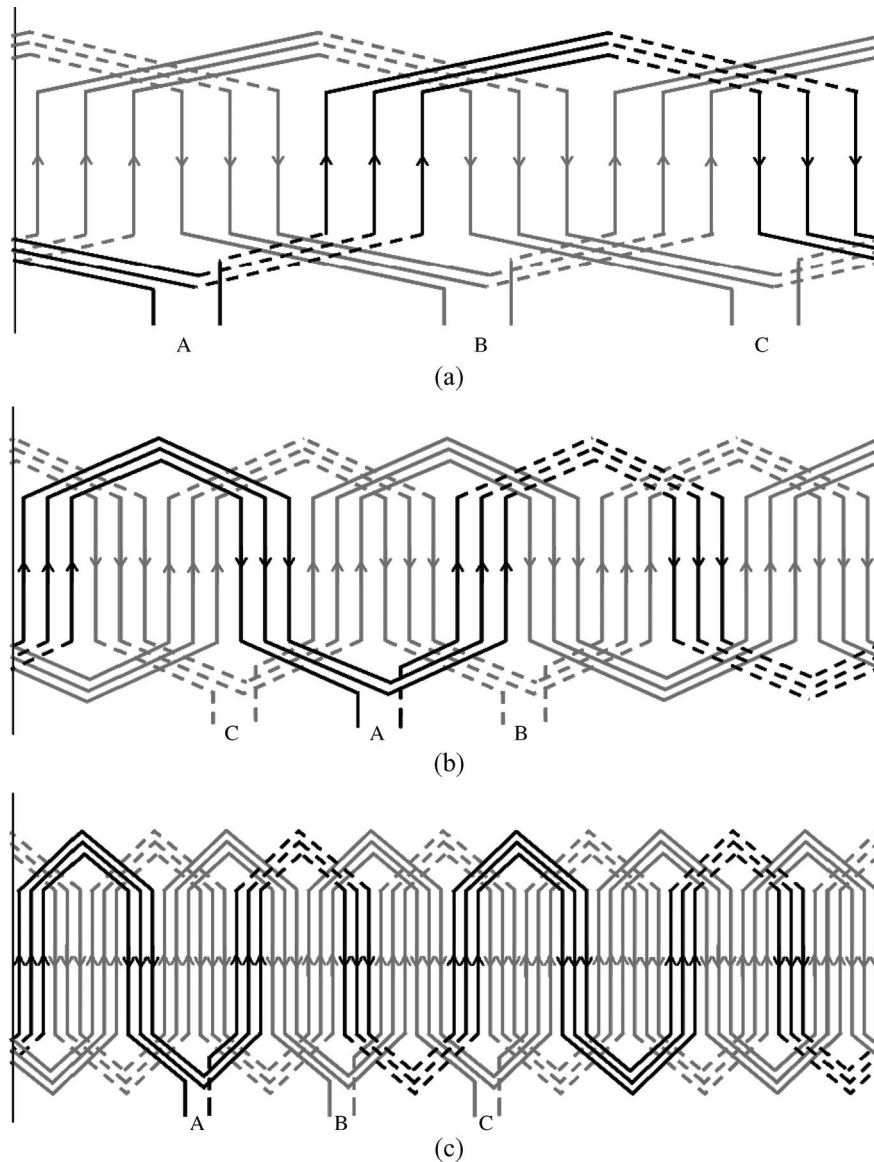


Fig. 2. Winding diagrams of (a) two-, (b) four-, and (c) eight-pole three-turn/pole designs. Solid line represents layer 1, and dashed line represents layer 2. Phase A is darkened for reference.

cobalt (SmCo) rings mounted in titanium housings failed upon surpassing 305 000 r/min of rotational speed [9]. This suggests that 2-mm-diameter magnets would not fail below ultrahigh speeds ( $> 1$  Mr/min) and could potentially be integrated with microfabricated air-bearing systems [11].

### B. Stator Design

Several stator geometries were designed in order to experimentally investigate the performances of ultraminiaturized PM generators as a function of the number of magnetic poles (two, four, and eight) and turns per pole (three and six). The key enabler for high power is to maximize the amount of copper in a given volume. Bar diagrams of three-phase multipole three-turn/pole stators are shown in Fig. 2 to give a better understanding of the winding patterns and pole dependences of the two-layer coil designs. To distinguish the phases, one phase (Phase A) is represented by a darker line than the other two. The solid and dashed lines represent the first and second copper

layers, respectively. These bar diagram schemes are still valid for six-turn/pole stators.

The radial conductors of a single phase are connected to each other by inner and outer end turns that cross over end turns of other phases. These design schemes are then arranged in a radial manner to operate along with rotating circular PM rotors. The actual geometries of the stator coils are determined by the given volume with the objective of minimizing the winding resistance by maximizing the amount of copper. Various patterns of the single-phase three-turn/pole surface-wound copper coils are shown in Fig. 3. The radial conductors shown in Fig. 3 and depicted by the solid vertical lines in Fig. 2 are of the thickness of the two copper layers.

Each phase of a three-phase generator spans 120 electrical degrees ( $\theta_e$ ). Thus, the mechanical angle  $\theta_m$ , which depends on the number of magnetic poles  $P$ , is given by

$$\theta_m = \frac{2}{p} \theta_e. \quad (1)$$

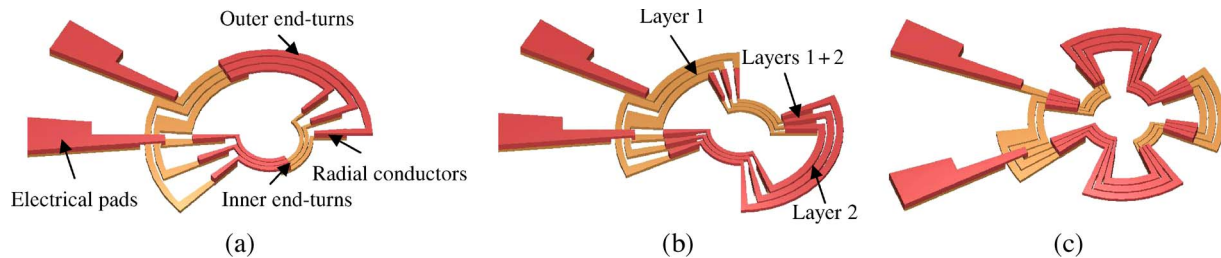


Fig. 3. Renderings of the single-phase three-turn/pole stator winding patterns for (a) two-, (b) four-, and (c) eight-pole designs.

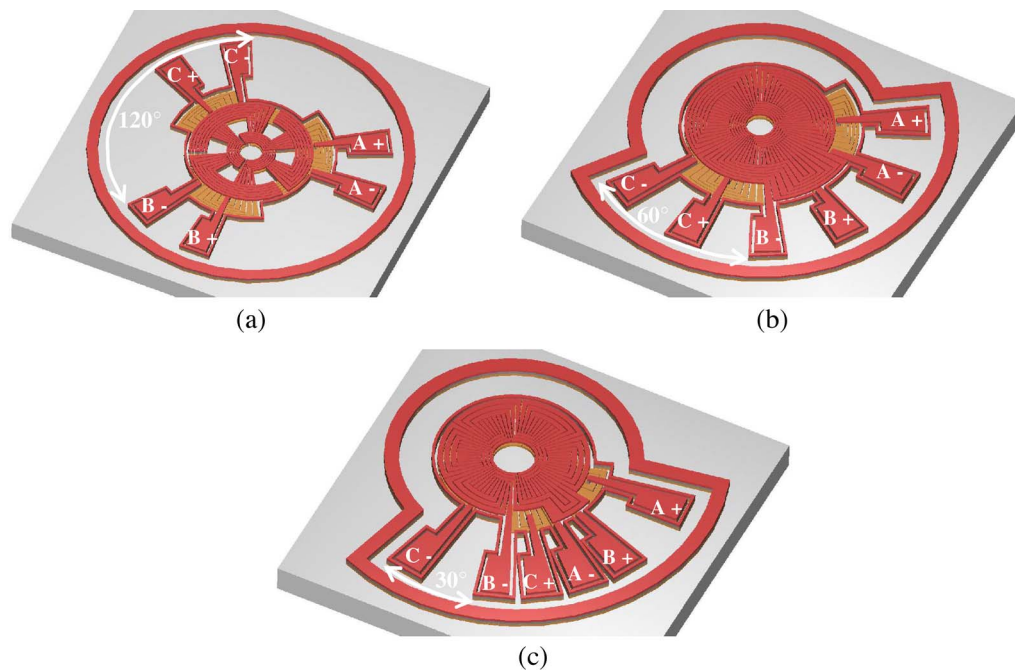


Fig. 4. Renderings of the stator winding patterns for (a) two-pole six-turn/pole, (b) four-pole six-turn/pole, and (c) eight-pole three-turn/pole designs.

TABLE I  
DESIGN CHARACTERISTICS OF THREE-PHASE 2-mm STATORS

Device number	Number of vias	Number of radial conductors	Width of radial conductors (at the ID – at the OD)	Minimum gap between adjacent radial conductors	Copper packing density
2-3C	21	18	38-73 $\mu\text{m}$	150 $\mu\text{m}$	21%
2-6	39	36	38-73 $\mu\text{m}$	10 $\mu\text{m}$	42%
4-3	3	36	38-73 $\mu\text{m}$	50 $\mu\text{m}$	42%
4-6	3	72	38-73 $\mu\text{m}$	10 $\mu\text{m}$	85%
8-3	3	72	38-73 $\mu\text{m}$	10 $\mu\text{m}$	85%

Accordingly, two-, four-, and eight-pole generators are designed using mechanical angles between the phases of 120°, 60°, and 30°, respectively. Fig. 4 shows some of the three-phase stator winding patterns. The devices are labeled using their corresponding numbers of poles and turns per pole. For example, a four-pole six-turn/pole stator is named “4-6.” The 2-3C design refers to a specific stator presented in [10].

For such PM machines, the stator active area, which captures the magnetic flux, is defined by the length and design of the radial conductors. The main design characteristics of each stator active area are summarized in Table I.

The number of radial conductors equals the number of phases multiplied by the numbers of turns and poles. The copper packing density is defined as the area occupied by the radial copper conductors over the total area bounded by

the outer and inner diameters of the radial conductors. Two-pole stators require more vias to avoid the end-turn conductors from overlapping each other. The inner and outer end turns of the various machines have a width of 50  $\mu\text{m}$  and a pitch of 60  $\mu\text{m}$  (interconductor gap = 10  $\mu\text{m}$ ).

### C. Rotor Design

The rotor consists of a titanium housing connected to a stainless steel shaft, a 0.5-mm-thick iron cobalt vanadium (FeCoV) disk, which acts as a back iron, and discrete pieces of either SmCo and NdFeB PMs. FeCoV (Hiperco 50) is selected as a back iron for its high saturation flux density ( $B_s \sim 2.4$  T) and high permeability ( $\mu_r > 3000$ ). The PMs are 0.5 mm thick and measure 1 mm in radial direction. Schematics of the magnetic

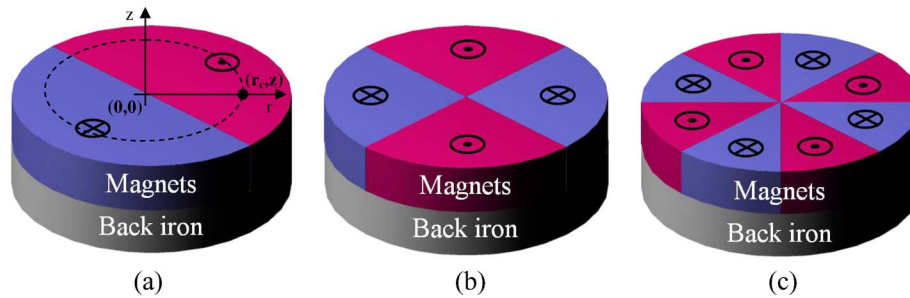


Fig. 5. Schematics of the different multipole rotors used in the 3-D magnetic modeling: (a) Two-, (b) four-, and (c) eight-pole rotors.

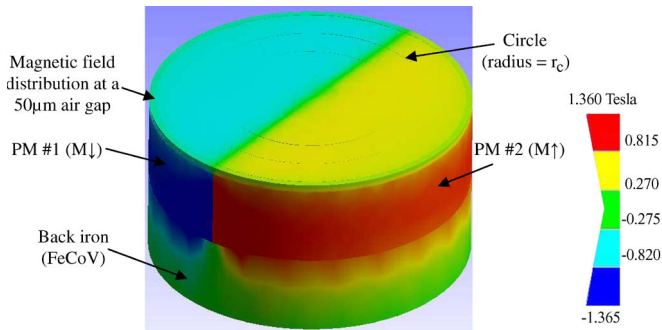


Fig. 6. Simulation results for two-pole rotors: 3-D view of the magnetic flux density at a 50- $\mu\text{m}$  air gap.

configurations of the two-, four-, and eight-pole rotors are shown in Fig. 5.

Even though the remanent magnetization of SmCo is approximately 25% lower than that of NdFeB ( $B_r = 11.5$  and 14 kG, respectively), its ability to withstand higher temperatures is attractive for such small pieces (Practical demagnetization temperatures are approximately  $T_{op} = 300$  °C and 80 °C, respectively). Indeed, the heat generated during the PM laser machining process can permanently degrade the magnetic material at the edges of the machined material, compromising the performance of the rotor.

Three-dimensional magnetic analyses of the 2-mm-diameter multipole rotors are carried out using finite element modeling. The variables and parameters used in the 3-D analyses are shown in Fig. 5(a). The material properties and the 3-D configurations introduced previously are used to model the distribution and intensity of the magnetic field as a function of the air gap  $z$  between the rotor and the stator copper windings. The PM pieces are modeled as perfectly magnetized elements. Fig. 6 shows the distribution of the magnetic flux density for two-pole rotors at the surface of a 50- $\mu\text{m}$  air gap. In addition, the field intensity has been evaluated as a function of the air gap. As expected, small air gaps must be maintained in order to benefit from a large magnetic field. Furthermore, the magnetic field is concentrated in a small portion of the volume of the FeCoV back iron, indicating that it does not saturate through the entire back iron thickness.

Simulation results are shown in Fig. 7. The field intensity of multipole rotors are shown for several air gaps in Fig. 7(a)–(c). The data are defined over a circle having a radius  $r_c$  that faces the center of the stator radial conductors and at a distance  $z$  of the rotor surface. The field intensity has also been simulated along the inner and outer boundaries of the radial conductors,

but did not show any significant variation. As a result, it is assumed that the field distribution is constant over the full length of the radial conductors. The coordinates on the  $x$ -axis correspond to the circle perimeter of a radius  $r_c$ . As the air gap increases, the magnetic field intensity decreases. At a 50- $\mu\text{m}$  air gap, the multipole rotors exhibit the same magnetic intensity. At larger air gaps, the intensity is higher for two-pole rotors compared to that of four- and eight-pole rotors, as shown in Fig. 7(d). This validates the design choice of using a low number of poles. Note that these simulations do not include any detrimental effects such as nonmagnetic zones between alternately poled magnets, due to degradation or other factors. The physical size of these nonmagnetic zones may become an appreciable fraction of the total magnet circumference in practical systems as miniaturization occurs, further reinforcing a design choice of lower number of poles. This effect will be discussed next in the context of experimental measurements.

### III. DEVICE FABRICATION

#### A. Stator Fabrication

The stator is a two-layer surface-wound copper coil micro-fabricated on top of a silicon wafer. First, a 15- $\mu\text{m}$ -thick copper layer is electrodeposited into a photoresist mold (NR9-8000 P, Futurrex). Second, an insulating layer of SU-8 epoxy is spin coated on top of the metal layer. Vias are opened in the SU-8, and the second layer of copper is electroplated through another mold of NR9-8000 photoresist. The process flow is similar to the one reported in [2], except that the dimensions of the layers differ. Fifty-two stators are batch fabricated on 75-mm-diameter silicon wafers. Fig. 8 shows scanning electron microscopy (SEM) images of the two electroplated copper layers that are 15 and 10  $\mu\text{m}$  thick, respectively. The SU-8 epoxy insulation layer between the two copper layers has been etched away for imaging purposes.

Individually diced stators are mounted on ceramic packages for electrical characterization, as shown in Fig. 9. The six stator terminals are connected directly to the package pads by wedge-bonding aluminum wires. No pretreatment of the electroplated surface was required to successfully perform the wire bonding.

#### B. PM Fabrication

The recent developments in electroplated and sputter-deposited PM technologies are very promising for power

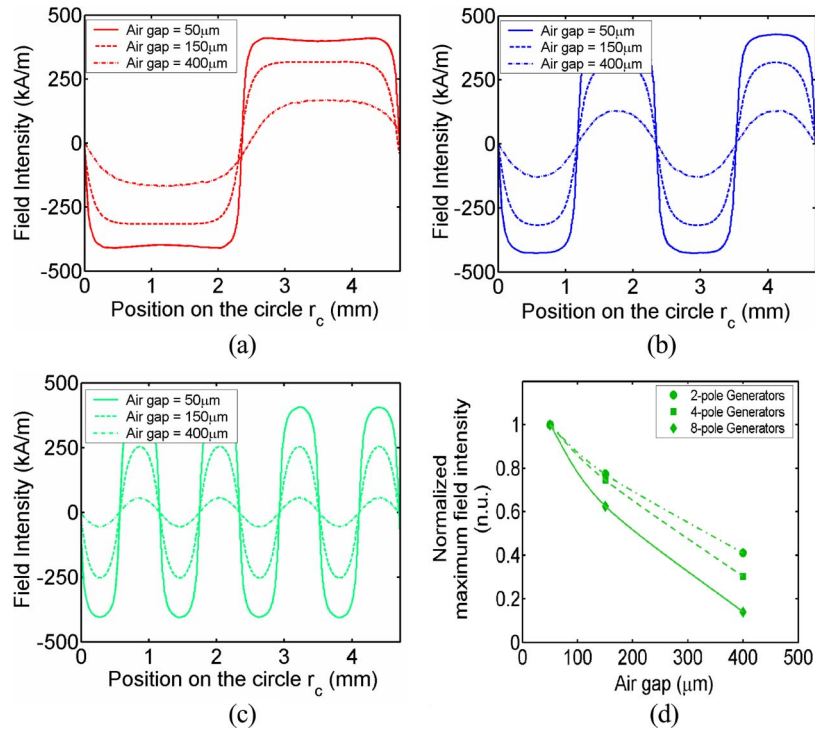


Fig. 7. Simulation results for multipole rotors. (a)–(c) Distribution of the field intensity along the circle  $r_c$  for several rotors and several air gaps. (d) Normalized maximum field intensity as a function of the air gap for several multipole rotor configurations.

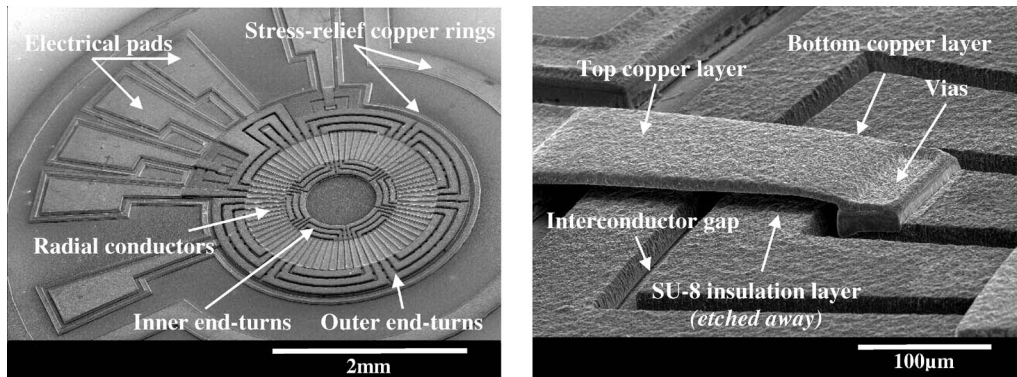


Fig. 8. SEM images of the fabricated stator windings: eight-pole three-turn/pole design.

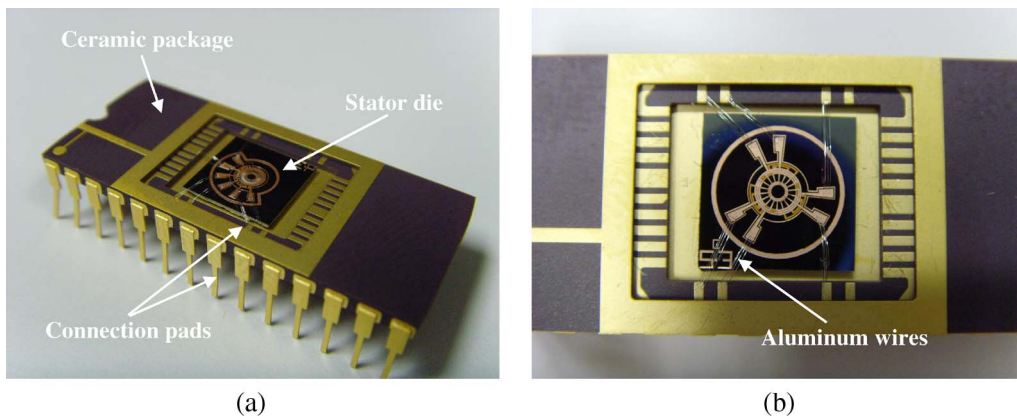


Fig. 9. Packaged stators. (a) View of the four-pole three-turn/pole device and (b) close-up on the two-pole three-turn/pole device.

MEMS devices. The magnetic performances achieved using these approaches are similar to the best bulk material characteristics [12]–[14]. Moreover, a technique to form

bonded micromagnets embedded in silicon has also been reported [15]. These various techniques can be very attractive for the fabrication of silicon-based PM generators comprising

TABLE II  
ND:YLF LASER PROCESS PARAMETERS

Laser characteristics		Process parameters	
Wavelength	1047 nm	Pulse repetition rate	1000
Pulse duration	180 ns		pulse per second
Beam diameter	100 $\mu\text{m}$	Cutting speed	1 mm/sec
Average power	$\sim 3.3$ W	Number of passes	3-5

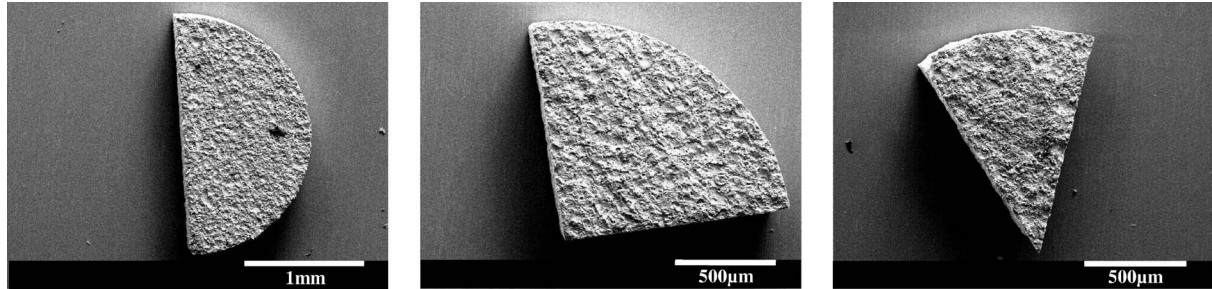


Fig. 10. SEM micrographs of laser machined SmCo magnet pieces used for (a) two-, (b) four-, (c) eight-pole rotors.

a silicon rotor with electroplated magnets that does not require manual assembly. Despite the advantages of batch fabrication and process integration, the thicknesses achieved with these approaches are still too thin (on the order of tens of micrometers) for our application. Thus, 0.5-mm sheets of high performance NdFeB and SmCo PMs are used to form the rotor magnetic components. SmCo magnets are also considered in this paper because they are much less susceptible to the machining-induced heat damage that may limit the performance of the more temperature-sensitive NdFeB material.

The PM material is first demagnetized by heating it above its Curie temperature and then machined using a 1047-nm Nd:YLF laser (Resonetics, Inc.). The laser characteristics and process parameters are detailed in Table II. The angular shape of the PM pieces is determined by the number of poles, as shown in Fig. 10. The PM pieces are then individually magnetized through the thickness using a discharge-capacitance magnetizer and assembled with respect to the alternating magnetic pole pattern.

#### IV. EXPERIMENTAL CHARACTERIZATION AND DISCUSSION

##### A. Magnetic Characterization

To verify that such small pieces were not considerably affected by the machining process, magnetic field measurements are performed on magnetized samples. By magnetically scanning the surface of the magnets, we were able to investigate the magnetic degradation near the edges of PM pieces. Two semi-circular PMs having a 1-mm radius are assembled as shown in Fig. 11. The samples are uniformly magnetized through the thickness. The measurements are obtained using a Hall effect sensor ( $0.2 \times 0.2$  mm active area) located 250  $\mu\text{m}$  above the sample surface. Experimentally, the  $z$ -component of the magnetic field is mapped across the entire surface of the sample. The results are shown in Fig. 12. For comparison, the magne-

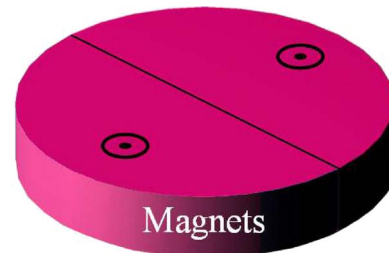


Fig. 11. Schematic of the uniformly magnetized two-piece magnet.

tization values of the magnetic sheets prior to laser machining were also measured. The laser-machined pieces present similar maximum values. With regard to the edge degradations, the SmCo samples do not exhibit a decrease in magnetic field at the border of the two pieces, while the NdFeB samples clearly show a magnetization drop, indicating that the material is degraded and, thus, less magnetic. However, a large area of the samples is fully magnetized, which confirms that laser machining of small-scale PMs is a feasible approach.

##### B. Stator Electrical Characterization

The single-phase winding resistances are modeled using 3-D finite element analysis as well as experimentally measured. Table II presents the results for the different geometries. The measured values are averaged over the three phases, which usually exhibit an imbalance on the order of a few milliohms. This is attributed to the nonuniform thickness of the electroplated copper. For the same reason, there are slight discrepancies between the simulated and measured values. The packaging adds a nonnegligible resistance, as indicated in the last column of Table III. The six-turn/pole surface-wound stator coils (2-6 and 4-6) have much higher resistances than their respective three-turn/pole devices (2-3C and 4-3) due to smaller cross-sectional areas of some electroplated features.

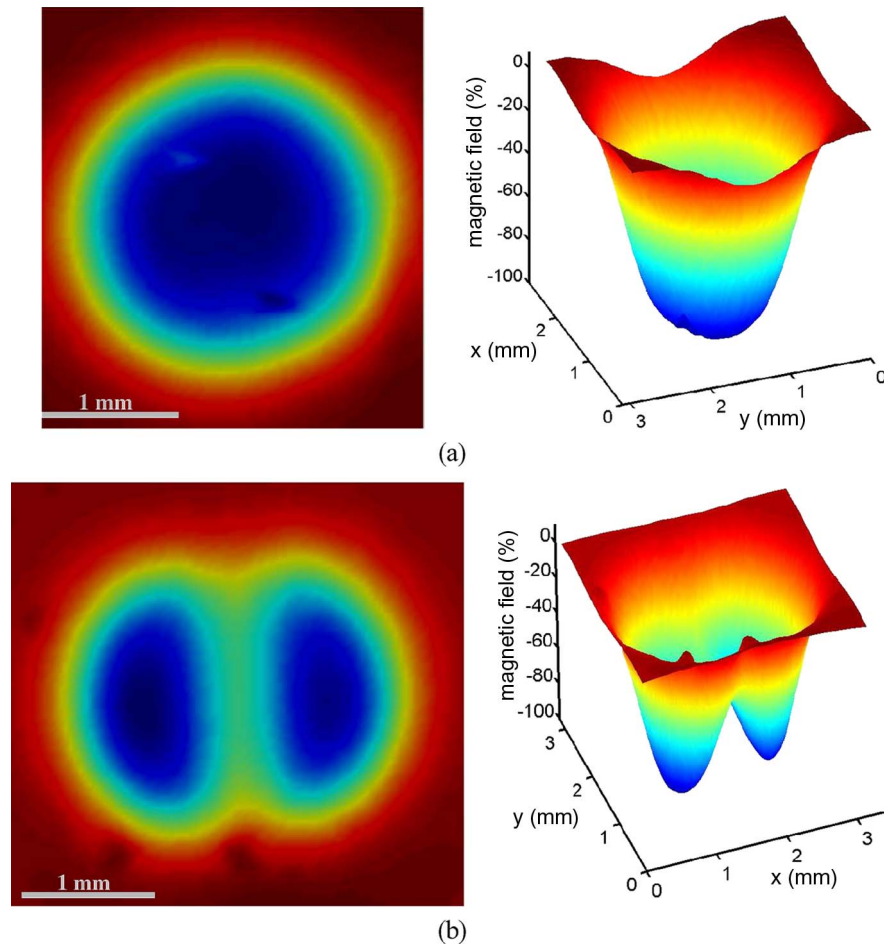


Fig. 12. Experimental magnetic maps of two-piece magnets: (a) SmCo and (b) NdFeB.

TABLE III  
ELECTRICAL CHARACTERIZATION OF THE DIFFERENT STATORS

Device number	Measured resistance (mΩ)	Simulated resistance (mΩ)	Error percentage	Measured resistance of the packaged device (mΩ)
2-3C	467	443	5%	573
2-6	1328	1192	11%	1442
4-3	505	527	4%	610
4-6	1530	1440	6%	1644
8-3	610	667	9%	720

C. Open-Circuit Voltage Measurements

To test the generator, the stator package is clamped on an *x-y-z* micropositioner stage that has a resolution of  $\pm 5 \mu\text{m}$  in all three directions. The shaft of the rotor is inserted into an off-the-shelf ball-bearing-supported air-driven turbine (Handpiece Parts and Products Inc., Orange, CA), which provides rotational speeds in excess of 390 000 r/min. A housing has been fabricated to hold the turbine in place and to provide inlet and outlet pressure ports. The experimental setup is shown in Fig. 13.

The stator is first set at a few hundred micrometers below the rotor, which is spinning at low speeds. *X-* and *Y-* alignments are achieved by monitoring the open-circuit voltage waveforms. The position of the stator is adjusted such that the voltage waveforms of the three phases are symmetric and sinusoidal, as shown in Fig. 14. At a rotational speed of 72 000 r/min

and a 450- $\mu\text{m}$  air gap, the 4-6 NdFeB microgenerator exhibits an output voltage waveform that has an amplitude of 18 mV ( $= 6.3 \text{ mV}_{\text{rms}}$ ) and an electrical frequency of 2.4 kHz. Once this procedure is completed, the air gap is decreased for electrical testing.

Open-circuit voltages measured from the different generators are shown in Fig. 15. For these experiments, the air gap between stators and rotors is set at  $50 \pm 10 \mu\text{m}$ . As expected, the generators present linear relationships between the rotor speed and the open-circuit voltage. The two-pole machines exhibit a 40% increase of output voltage over the similar machines previously reported [9]. This is solely due to better magnetization of the PM pieces, which are now fully magnetized. The six-turn/pole generators demonstrate approximately two times higher open-circuit voltages than the three-turn/pole devices, using the same

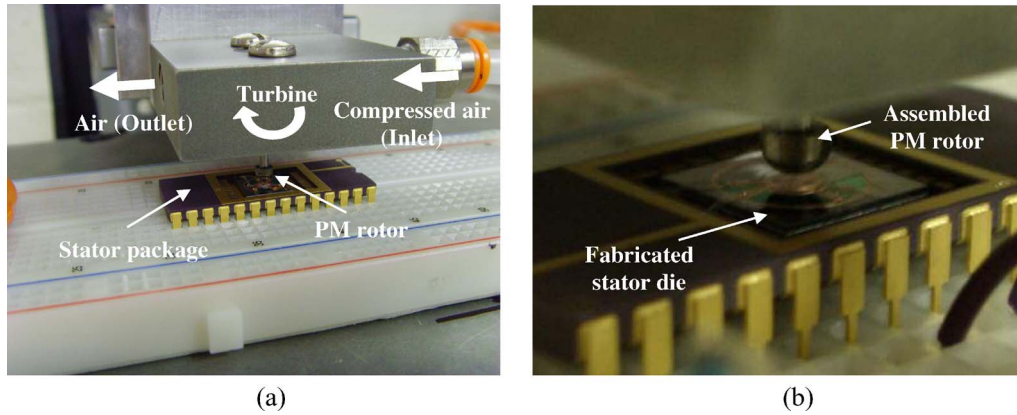


Fig. 13. (a) View of the experimental setup. (b) Close-up on the microgenerator. The packaged stator is plugged into a solderless board for electrical characterization.

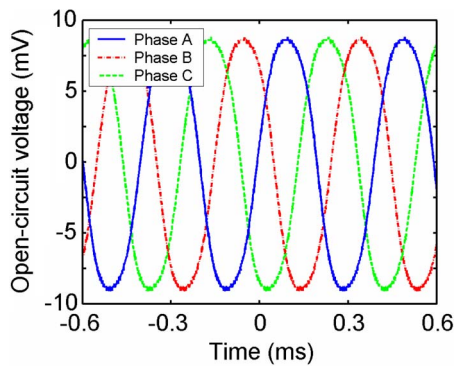


Fig. 14. Open-circuit voltage waveforms of the three phases of the 4-6 NdFeB microgenerator during adjustment phase.

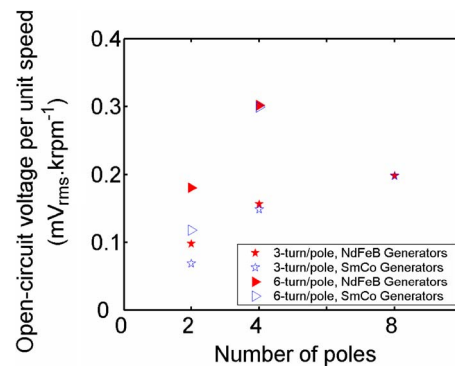


Fig. 16. Open-circuit voltage per unit speed as a function of the number of magnetic poles.

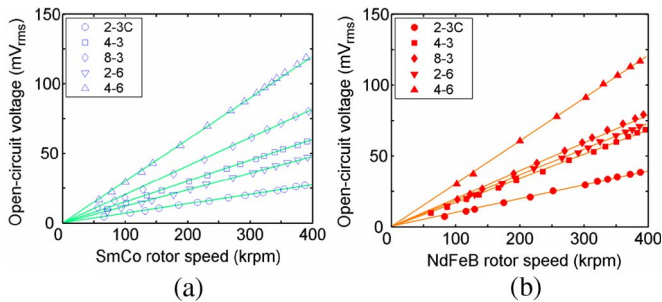


Fig. 15. Open-circuit voltage measurements as a function of the rotor speed using (a) SmCo and (b) NdFeB rotors.

PM rotors. A maximum open-circuit voltage of  $120 \text{ mV}_{\text{rms}}$  has been extracted out of the 4-6 generators, using either SmCo or NdFeB rotors.

Furthermore, two-pole NdFeB generators show superior performance to two-pole SmCo generators on the order of 45%. Nevertheless, this difference does not remain valid for four- and eight-pole machines as NdFeB and SmCo devices present similar results, as shown in Fig. 16. Even though the remanent magnetization of NdFeB PMs is higher than that of SmCo, larger volumes of nonmagnetic material at the edges of the laser-machined pieces lower the overall magnetic flux and, thus, the output voltage. In addition, the difficulty of assembling very small PM pieces may induce lateral gaps between each pole, which also affects the performance of the machines.

Fig. 17 shows the measurements of the open-circuit voltage per unit speed as a function of the air gap, as well as the normalized data. As predicted by the simulations shown in Fig. 7(d), eight-pole machines are less efficient for large air gaps. Experimental trends are also confirmed by the magnetic simulations. The open-circuit voltage decays as the gap increases. This suggests that greater output voltage could be achieved if air gaps smaller than  $50 \mu\text{m}$  between the stator and the high-speed PM rotor could be maintained. However, tradeoffs between performance and stability must be taken into account depending on the targeted applications. At very high speeds, the bearing stability is crucial to avoid severe wobbling of the rotor. In addition, the system will be more sensitive to external vibrations, which may cause the rotor to crash into the stator. With larger air gaps, external perturbations will have less of an effect on the system.

Fig. 18 shows the open-circuit voltage as a function of electrical frequency. The electrical frequency range increases as the number of poles increases. For low-frequency applications, two-pole machines are desired as they deliver higher open-circuit voltages.

#### D. Power Generation

By analyzing the open-circuit voltage of the PM generators, one can extract the estimated three-phase output power at the point of maximum transfer using (2) and (3). As

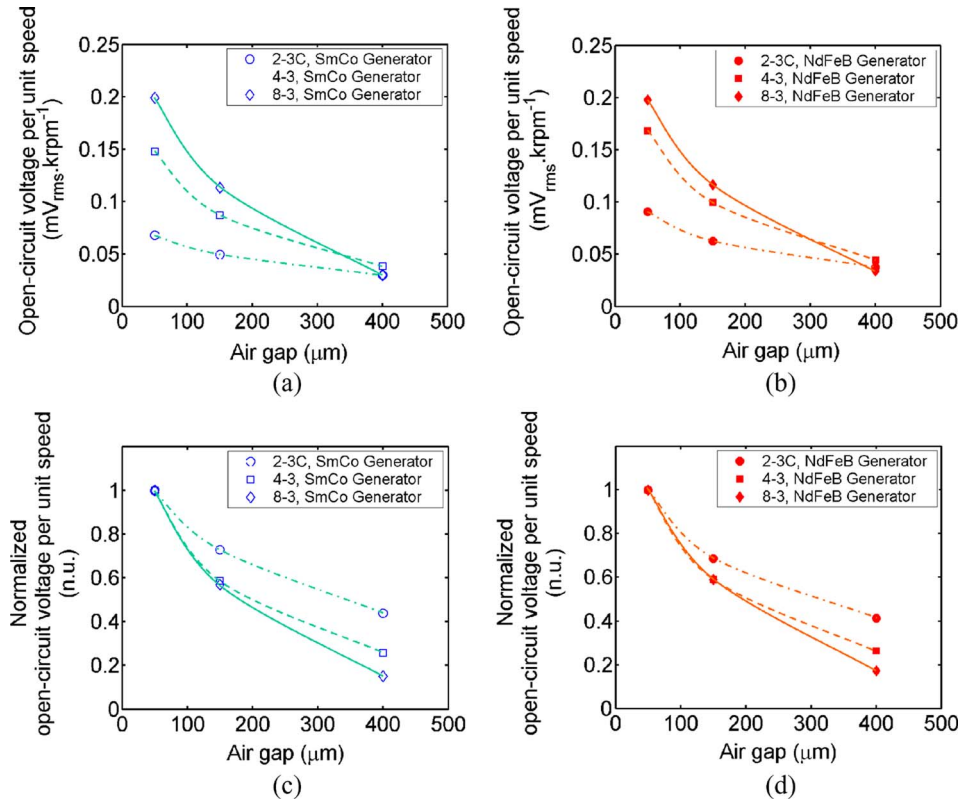


Fig. 17. Open-circuit voltage per unit speed as a function of the air gap for three-turn/pole generators using (a) SmCo and (b) NdFeB rotors. (c) and (d) Show their respective normalized values.

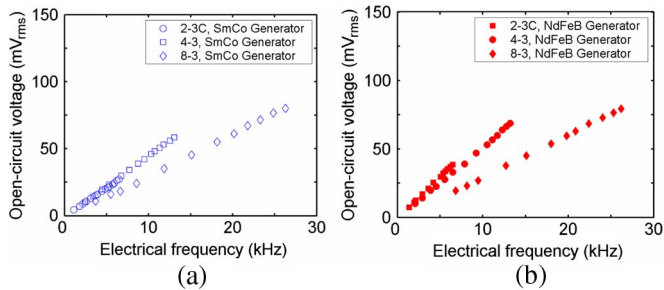


Fig. 18. Open-circuit voltage as a function of the electrical frequency: (a) SmCo and (b) NdFeB generators.

defined by Thevenin’s theorem, the maximum power transfer occurs for

$$R_{load} = R_{source} = R_w + 2 \times R_{pin} + 2 \times R_c. \quad (2)$$

$R_{load}$  is the external load resistance, and  $R_{source}$  is the coil resistance and includes the winding resistance  $R_w$ , the package resistance  $R_{pin}$ , and the resistance of the aluminum wire connections  $R_c$ . As a result, the three-phase output power can be calculated using the following:

$$P_e = \frac{3}{4} \times \frac{V_{oc}^2}{(R_w + 2 \times R_{pin} + 2 \times R_c)}. \quad (3)$$

$P_e$  is the output electrical power, and  $V_{oc}$  is the root-mean-square (rms) open-circuit voltage. The factor three comes from the three phases, and the coefficient 1/4 assumes matched load conditions.

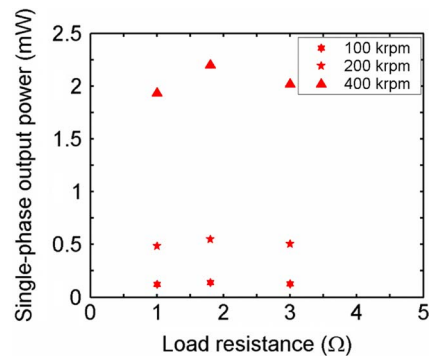


Fig. 19. Single-phase output power delivered by the 4-6 NdFeB generator as a function of the load resistance for various rotational speeds.

Various load resistances are connected to one phase of the machines to demonstrate ac power generation. The rms voltage is measured across the resistance and used to calculate the electrical power. Fig. 19 shows the single-phase output power from the 4-6 NdFeB generator measured across a variety of loads for several rotational speeds. As expected, the output power is maximized under matched load conditions ( $R_{source} = R_{load} \sim 1.8 \Omega$ ).

As shown in Fig. 20, 4-6 NdFeB machines generate a maximum single-phase output power of 2.2 mW at a measured rotational speed of 392 000 r/min across a resistive load of 1.8  $\Omega$ . This corresponds to a three-phase output power of 6.6 mW. The dots represent the measured single-phase power, and the line indicates calculated data from (3). Note that the calculated data underestimate the direct power measurements

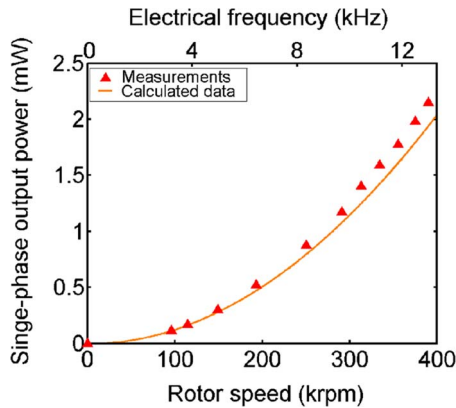


Fig. 20. Single-phase electrical power as a function of the rotor speed and electrical frequency for 4-6 NdFeB generators.

by approximately 10%. This discrepancy can be attributed to a small variation in the stator-rotor gap during the experiment.

The air turbine performance limits characterization at higher speeds, but a projected output power of 40 mW could be achieved at 1 Mr/min, neglecting potential losses in the stator coils such as eddy currents and heat-related degradation. Moreover, we have demonstrated that design choices, such as the number of poles and turns per pole, are critical for the performance of miniature generators.

Finally, the performance of the PM generators reported in this paper could be improved by integrating magnetic laminated stator cores. By adding a stator back iron to the machine, the overall magnetic reluctance would decrease, which in turn would increase the output voltage of the device. An appropriate design of the laminations will decrease the generation of eddy currents in the stator back iron and increase the efficiency of the mechanical-to-electrical energy conversion.

## V. CONCLUSION

Ultraminiaturized axial-flux synchronous PM generators were designed and fabricated by combining microfabrication techniques and laser micromachining. Different designs and materials were tested, such as the use of NdFeB and SmCo PMs, as well as several pole and turn configurations. Magnetic simulations of multipole PM rotors were carried out using finite element analysis. The devices were magnetically and electrically characterized. In addition, an off-the-shelf air-driven turbine was used to spin the rotor at high speeds and measure the electrical performance of the machines. The experimental characterizations suggest that a higher number of magnetic poles results in a higher degradation of the magnetic performance of the small-scale PMs. Consequently, a low number of poles should be favored when designing ultraminiaturized PM generators. The open-circuit voltage of the machines increases linearly with the number of turns. Even though the coil resistance does not have a linear relationship with the number of turns per pole due to smaller cross-sectional areas, it is still advantageous to maximize the number of turns in a given volume, because the power is proportional to the square of the voltage, while inversely proportional to the resistance. Across a resistive load, four-pole six-turn/pole NdFeB microgenerators demonstrated

a maximum output power of 6.6 mW at a rotational speed of 392 000 r/min. For an active volume of 3.4 mm<sup>3</sup> (thickness = 1.08 mm, OD = 2 mm), the corresponding power density is about 1.95 W · cm<sup>-3</sup>. These promising results indicate that ultraminiaturized magnetic generators are a feasible approach for the generation of milliwatt-scale power. While maintaining a comparable level of power density with other MEMS-based PM generators reported in [7], we were able to further downscale these generators and investigate the limitations of miniaturization. Future efforts will be focused on the optimization of the stator geometries and the addition of a laminated stator back iron for higher power densities. Furthermore, the development of an integrated system that includes a ball-bearing-supported microturbine is also considered.

## ACKNOWLEDGMENT

The authors would like to thank R. H. Shafer from the Georgia Institute of Technology for his assistance regarding the laser machining of PMs and Prof. J.-C. Portal from the National Institute of Applied Sciences (INSA, Toulouse, France) for the valuable discussions related to this paper.

## REFERENCES

- [1] S. Das, D. P. Arnold, I. Zana, J.-W. Park, M. G. Allen, and J. H. Lang, "Microfabricated high-speed axial-flux multiwatt permanent-magnet generators—Part I: Modeling," *J. Microelectromech. Syst.*, vol. 15, no. 5, pp. 1330–1350, Oct. 2006.
- [2] D. P. Arnold, S. Das, J.-W. Park, I. Zana, J. H. Lang, and M. G. Allen, "Microfabricated high-speed axial-flux multiwatt permanent-magnet generators—Part II: Design, fabrication, and testing," *J. Microelectromech. Syst.*, vol. 15, no. 5, pp. 1351–1363, Oct. 2006.
- [3] H. Raisigel, O. Cugat, and J. Delamare, "Permanent magnet planar micro-generators," *Sens. Actuators A, Phys.*, vol. 130/131, pp. 438–444, Aug. 2006.
- [4] S. A. Jacobson and A. H. Epstein, "An informal survey of power MEMS," in *Proc. Int. Symp. Micro-Mech. Eng.*, 2003, pp. 513–520.
- [5] A. S. Holmes, G. Hong, and K. R. Pullen, "Axial-flux permanent magnet machines for micropower generation," *J. Microelectromech. Syst.*, vol. 14, no. 1, pp. 54–62, Feb. 2005.
- [6] C. T. Pan and T. T. Wu, "Development of a rotary electromagnetic microgenerator," *J. Micromech. Microeng.*, vol. 17, no. 1, pp. 120–128, Jan. 2007.
- [7] D. P. Arnold, "Review of microscale magnetic power generation," *IEEE Trans. Magn.*, vol. 43, no. 11, pp. 3940–3951, Nov. 2007.
- [8] D. P. Arnold, F. Herrault, I. Zana, P. Galle, J.-W. Park, S. Das, J. H. Lang, and M. G. Allen, "Design optimization of an 8-watt, microscale, axial-flux, permanent-magnet generator," *J. Micromech. Microeng.*, vol. 16, no. 9, pp. S290–S296, Sep. 2006.
- [9] D. P. Arnold, Y.-H. Joung, I. Zana, J.-W. Park, S. Das, J. H. Lang, D. Veazie, and M. G. Allen, "High-speed characterization and mechanical modeling of microscale, axial-flux, permanent-magnet generators," in *13th Int. Conf. Solid-State Sens., Actuators, Microsyst. Tech. Dig.*, Jun. 2005, vol. 1, pp. 701–704.
- [10] F. Herrault, C.-H. Ji, R.H. Shafer, S.-H. Kim, and M. G. Allen, "Ultraminiaturized milliwatt-scale permanent magnet generators," in *Proc. 14th Int. Conf. Solid-State Sens., Actuators, Microsyst., Tech. Dig. (Transducers)*, Jun. 2007, vol. 1, pp. 899–902.
- [11] A. Epstein *et al.*, "Power MEMS and microengines," in *9th Int. Conf. Solid-State Sens., Actuators, Microsyst. Tech. Dig.*, Jun. 1997, vol. 2, pp. 753–756.
- [12] T. Budde and H. H. Gatzel, "Magnetic properties of an SmCo/NiFe system for magnetic microactuators," *J. Magn. Magn. Mater.*, vol. 272–276, pp. 2027–2028, May 2004.
- [13] N. M. Dempsey, A. Walther, F. May, D. Givord, K. Khlopkov, and O. Gutfleisch, "High performance hard magnetic NdFeB thick films for integration into micro-electro-mechanical systems," *Appl. Phys. Lett.*, vol. 90, no. 9, pp. 092 509-1–092 509-3, Feb. 2007.

- [14] A. Walther, D. Givord, N. M. Dempsey, K. Khlopkov, and O. Gutfleisch, "Structural, magnetic, and mechanical properties of 5  $\mu\text{m}$  thick SmCo films suitable for use in microelectromechanical systems," *J. Appl. Phys.*, vol. 103, no. 4, pp. 043 911-1–043 911-5, Feb. 2008.
- [15] B. Bowers, J. Agashe, and D. P. Arnold, "A method to form bonded micromagnets embedded in silicon," in *14th Int. Conf. Solid-State Sens., Actuators, Microsyst. Tech. Dig.*, Jun. 2007, vol. 2, pp. 1581–1584.



**Florian Herrault** received the B.S. and M.S. degrees in physics and materials science from the National Institute of Applied Sciences, Toulouse, France, in 2003 and 2005, respectively. He is currently working toward the Ph.D. degree in electrical engineering at l'Ecole Doctorale de Toulouse, and he is conducting research at the School of Electrical and Computer Engineering, Georgia Institute of Technology, Atlanta. His Ph.D. research mainly focuses on developing gas-driven microscale generators.

His current research interests include electromagnetic actuators, small-scale power generation systems, and 3-D MEMS fabrication.



**Chang-Hyeon Ji** received the B.S. and M.S. degrees in electrical engineering and the Ph.D. degree in electrical engineering and computer science from Seoul National University, Seoul, Korea, in 1995, 1997, and 2001, respectively. His doctoral dissertation concerned the design, fabrication, and testing of electromagnetic micromirrors for microphotonic applications.

He was with LG Electronics Institute of Technology, Seoul, from 2001 to 2006, where he developed microactuators for various types of applications including optical communications and scanning laser displays. He is currently a Postdoctoral Fellow with the School of Electrical and Computer Engineering, Georgia Institute of Technology, Atlanta. His current research interests include micro power generation, micromachined components and interconnection technology for high-power electronics, and BioMEMS.



**Mark G. Allen** (M'89–SM'04) received the B.A. degree in chemistry, the B.S.E. degree in chemical engineering, and the B.S.E. degree in electrical engineering from the University of Pennsylvania, Philadelphia, and the S.M. and Ph.D. degrees from the Massachusetts Institute of Technology, Boston.

Since 1989, he has been with the faculty of the School of Electrical and Computer Engineering, Georgia Institute of Technology, Atlanta, where he currently holds the rank of Regents' Professor and the J.M. Pettit Professorship in Microelectronics, as well as a joint appointment with the School of Chemical and Biomolecular Engineering. He also holds the position of Senior Vice Provost for Research and Innovation, and is charged with overseeing Georgia Tech's interdisciplinary research centers, managing Georgia Tech's sponsored research portfolio, and guiding the commercialization of Georgia Tech research results and intellectual property. He is the Editor-in-Chief of the *Journal of Micromechanics and Microengineering*. His current research interests are in the field of microfabrication and nanofabrication technology, with emphasis on new approaches to fabricate devices with characteristic lengths in the micro- to nanoscale from both silicon and nonsilicon materials. Examples include micromagnetics, high-temperature sensors, small-scale power generation, biofluidic microvasculatures and implantable microsensors, and the use of microstructures to create nanostructures.

Dr. Allen was the Co-Chair of the 1996 IEEE/ASME Microelectromechanical Systems Conference.